Correlation Technologies for Emerging Wireless Applications

Sidina Wane, Fabien Ferrero, Thanh Vinh Dinh, Damienne Bajon, Lionel Duvillaret, Gwenaël Gaborit, Vincent Huard

electronics

MDPI

Article

Correlation Technologies for Emerging Wireless Applications

Sidina Wane [1,*], Fabien Ferrero [2], Thanh Vinh Dinh [1], Damienne Bajon [1], Lionel Duvillaret [3], Gwenaël Gaborit [3] and Vincent Huard [4]

[1] eV-Technologies, 2 Esplanade Anton Philips, 14460 Colombelles, France; thanh-vinh.dinh@ev-technologies.com (T.V.D.); damienne.bajon@ev-technologies.com (D.B.)
[2] LEAT-CREMANT (Laboratory of Electronics Antennas and Telecommunications)—UMR 7248, 06903 Sophia Antipolis, France; fabien.ferrero@unice.fr
[3] Kapteos SAS, Bât. Cleanspace 354 voie Magellan, Z.A. Alpespace, 73800 Sainte-Hélène-du-Lac, France; lionel.duvillaret@kapteos.com (L.D.); gwenael.gaborit@kapteos.com (G.G.)
[4] Dolphin-Design France, 38240 Meylan, France; vincent.huard@dolphin.fr
* Correspondence: sidina.wane@ev-technologies.com

Abstract: In this article, we introduce correlation technologies both at RF/mmWave and baseband frequencies. At RF and mmWave frequencies, power-spectra and energy-spectra metrics are introduced for measuring the power-density of mobile devices and systems. New *ASIC-embedded smart connectors* are developed for bringing correlation-based signal processing close to antenna modules. At baseband frequencies, DSP-based convolutional accelerators are proposed for fast and accurate measurement of EVM (error vector magnitude) using correlation technologies. Porting of the DSP-based convolutional accelerators into advanced fully depleted silicon-on-insulator (FDSOI)-based ASIC platforms for co-integration with adaptive RF/mmWave front-end modules will enable real-time extraction of *auto-correlation* and *cross-correlation* functions of stochastic signals. Perspectives for optically synchronized interferometric-correlation technologies are drawn for accurate measurements in noisy environments of stochastic EM fields using power-spectra and energy-spectra metrics. Adoption of correlation technologies will foster new paradigms relative to interactions of humans with smart devices and systems in randomly fluctuating environments. The resulting new paradigms will open new possibilities in communication theory for properly combining and reconciling information signal theory (*Shannon information-based entropy*) and physical information theory (*statistical-physics-based entropy*) into a unified framework.

Keywords: correlation technologies; secure quantum sensing; power-density; energy-density; entropy; interferometric synchronization; OTA-testing; electro-optical probing; EVM

Citation: Wane, S.; Ferrero, F.; Dinh, T.V.; Bajon, D.; Duvillaret, L.; Gaborit, G.; Huard, V. Correlation Technologies for Emerging Wireless Applications. *Electronics* **2022**, *11*, 1134. https://doi.org/10.3390/electronics11071134

Academic Editor: Giovanni Crupi

Received: 5 January 2022
Accepted: 26 February 2022
Published: 2 April 2022

1. Introduction

Field–Field correlation [1–4] functions (FF-CF), in revealing unified information about the signals to which they refer and the space through which the radiation has propagated, provide solid foundations for bridging modeling and measurement into a consistently complementary framework. In a broad range of applications, including ultrasonics [5], under-water acoustics [6], geophysics [7], it is observed that the Green's function can be retrieved by cross-correlating fluctuations recorded at two locations. For structures that are not invariant under time reversal, it is demonstrated [8] that the fluctuations must be excited by volume sources in order to satisfy the energy balance (equipartitioning) that is required to retrieve the Green's function. The extracted auto-correlation and cross-correlation functions can be linked to the general theory of coherence [9,10].

In this contribution, we introduce power-density-based metrics using advanced auto and cross-correlation technologies for OTA testing of wireless mobile devices. The use of correlation-based energy metrics is foreseen to foster new measurement solutions for accurately assessing equivalent isotropically radiated power (EIRP) and the total radiated

power (TRP), which are of relevance to standardization bodies for establishing maximum permissible transmitted power of wireless mobile devices in the mmWave frequency range. The requirements and challenges of OTA tests, including the need for unified measurement and modeling platforms, are highlighted in several contributions [2,4]. New *ASIC-embedded smart connectors* are developed for bringing correlation-based signal processing close to antenna modules. At baseband frequencies, perspectives are drawn for DSP-based convolutional accelerators toward fast and accurate measurement of EVM using correlation technologies.

The originality of the proposed technology solutions includes the following attributes:

- Use of correlation functions for energy and power-density-based metrics testing of wireless devices.
- Minimally invasive electro-optical probes for very near-field sensing of EM fields in noisy environments.
- Cognition-ready signal processing solutions using SinC [Cardinal-Sine] convolutional algorithms for OTA testing.

The proposed correlation technologies for overcoming the limitations of classical interferometers offer new solutions for measuring arbitrary correlations functions of stochastic fields. Perspectives for optically synchronized interferometric-correlation technologies are drawn for accurate measurements in noisy environments of stochastic electromagnetic fields using power-spectra and energy-spectra metrics.

2. Correlation Functions for Stochastic Fields

We introduce correlation technologies implemented using integrated front-end modules for effective, simple, and robust methods for extracting *correlation functions* defined in (1) as $\Gamma(x, x')$ where the angle brackets refer to an average over the ensemble of realizations of the (dimensionless) analytic signal $E(x)$:

$$\Gamma(x, x') = \langle E^*(x)E(x')\rangle \tag{1}$$

In Figure 1a, an adaptive front-end module (AFEM), implementing a unified RF/mmWave, and baseband correlation technologies are presented. The front-end module provides an adjustable 80 dB dynamic range for efficiently characterizing user-equipment (UE) mobile devices using power-density and energy-density metrics. The AFEM is combined with Mosaic-based array technologies built using wafer-level chip-scale-packaging (WLCSP) compliant with antenna-in-package (AiP) solutions. The resulting AFEM-AiP co-design enables radical vision: replacing antenna arrays with energy-efficient and affordable 'Smart Integrated Electromagnetic Emitting and Receiving surfaces and volumes', conformal to the shape of the object they are installed on.

Assuming fully coherent EM distributions, the CF can be factorized to yield the field amplitude:

$$|E(x)| = \sqrt{\Gamma(x, x)} \tag{2}$$

The phase of the field can be extracted relative to a constant phase reference φ_{ref}:

$$Arg[E(x)] = \tan^{-1}\left[\frac{Im(\Gamma(x, x'))}{Re(\Gamma(x, x'))}\right] + \varphi_{ref} \tag{3}$$

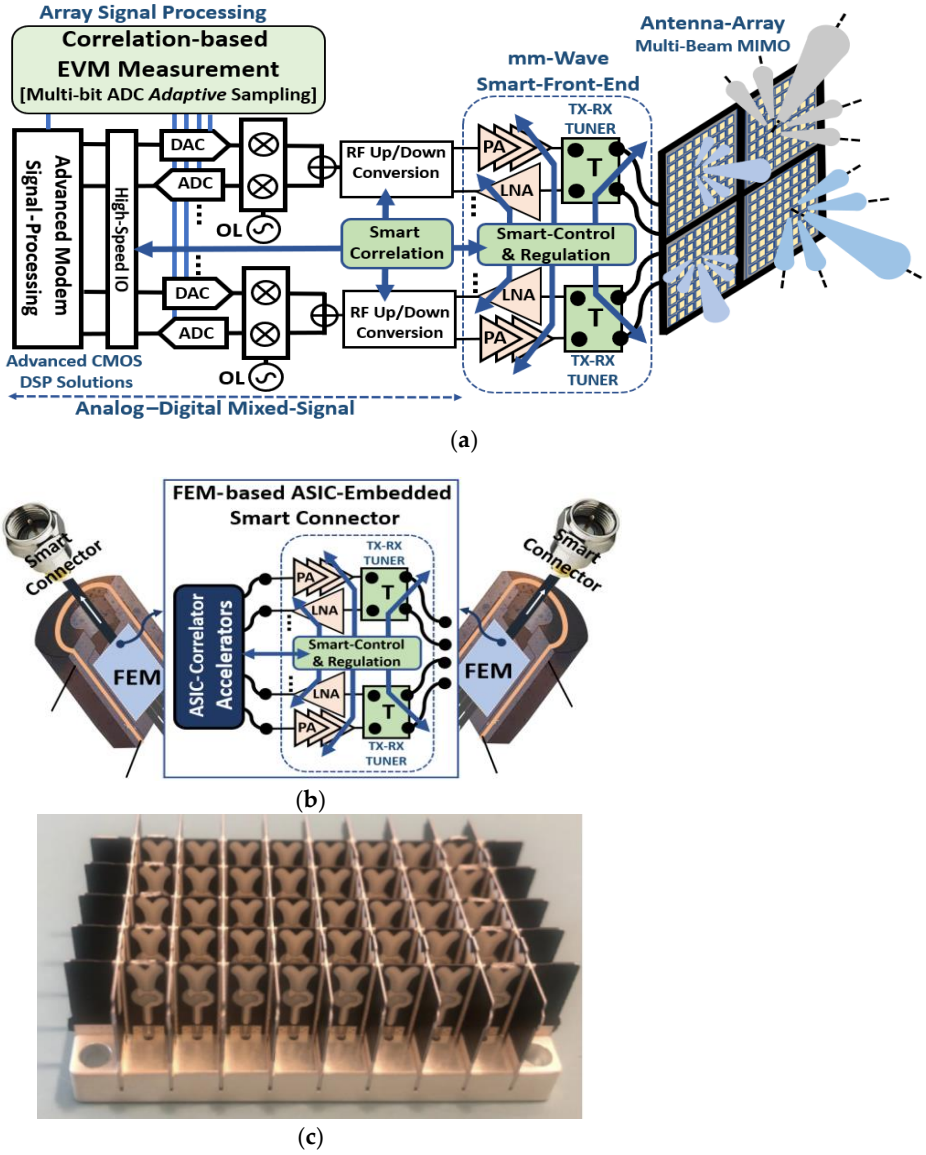

Figure 1. (**a**) Wireless adaptive front-end modules including advanced auto and cross-correlation signal processing and multi-beam MIMO antennas. (**b**) Smart connectors with embedded front-end modules. (**c**) Dual-polarization probe-array using Vivaldi antennas.

For random fields, it is required to deal with energy and power spectra [2] through the extraction of stochastic correlation functions. Born and Wolf [10] have indicated possibilities to extract correlation functions with the paradigm of two-beam interferometers, Young's double slit, by measurement of the fringe visibility and position for a large number of slit positions and separations. Interferometric techniques have been mainly aimed at a partial reconstruction of the field based on a priori assumptions such as space-shift invariance of the correlation functions or complete coherence of the source. Such measurement setup is thought to be challenging and ill-suited to the measurement of arbitrary correlation functions. Key coherence related quantities such as the temporal field correlation function $g(\tau)$ referenced as first-order correlation function:

$$g^{(1)}(\tau) = \frac{\langle E^*(t)E(t+\tau)\rangle}{\langle I(t)\rangle} \tag{4}$$

With $I(t) = \langle E^*(t)|E(t)\rangle$ being the intensity associated with the field $E(t)$. From the first-order correlation function, coherence-based quantities such as optical spectrum,

frequency noise power spectral density (PSD) can be measured. Nevertheless, following the work of Glauber [11], it is established that full characterization of the coherence properties of a light source requires the measurement of the correlation functions $g^{(k)}$ at all orders k. Thus, the second-order temporal correlation function, also called temporal intensity correlation function, can be derived as:

$$g^{(2)}(\tau) = \frac{\langle I(t)I(t+\tau)\rangle}{\left\langle I(t)^2\right\rangle} \tag{5}$$

For fields that present properties of Gaussian processes, it happens [12,13] that the correlation functions $g^{(k)}(\tau)$ are related to each other. In the case of a spatially-coherent polarized chaotic field, the second-order correlation function $g^{(2)}(\tau)$ is related to the modulus of the temporal first-order correlation function $g^{(1)}(\tau)$ as follows:

$$g^{(2)}(\tau) = 1 + \left|g^{(1)}(\tau)\right|^2 \tag{6}$$

Equation (6) is commonly called the Siegert relation. In [12,13] the challenges of measuring both field and intensity correlations at the same time are addressed for a direct assessment of the Siegert relation highlighting the conditions where the relation fails. In the situations where the Siegert relation fails, measuring $g^{(2)}(\tau)$ convey quantum effects and helps in distinguishing different types of sources in the perspectives of properly classifying and reconstructing them in practical tomographic and imaging applications. An implication of Equation (6) is that there is an excess of intensity correlation at zero delays, $g^{(2)}(0) > g^{(2)}(\tau \to \infty) = 1$ following in reference to "*photon bunching*" or the "*Hanbury Brown and Twiss*" effect.

For deterministic noise power density distribution, the challenge of energy detection of unknown signals in the presence of noise is discussed in [12]. For stochastic signals, it is established that numerical values of noise amplitudes cannot be specified. Thus, for modeling and measuring stochastic signals, it is required to deal with energy and power spectra through the extraction of correlation functions. The energy density can be written as the sum of electric and magnetic energy densities [14]:

$$W(\rho) = W_E(\rho) + W_H(\rho) \tag{7}$$

$$W_E(\rho) = \frac{\varepsilon}{2}|E(\rho)|^2 \; and \;\; W_H(\rho) = \frac{\mu}{2}|H(\rho)|^2 \tag{8}$$

The correlation function of the electric or magnetic field is defined as:

$$C_X^{FF} \equiv \frac{X(\rho_1)\cdot X^*(\rho_2)}{\sqrt{\langle|X(\rho_1)|^2\rangle\langle|X(\rho_2)|^2\rangle}} \tag{9}$$

where $\langle X\rangle$ refers to ensemble average (expectation) applied to stochastic variable X and * stands for complex conjugate. In (9) the square-root in the denominator is introduced for normalization purposes without loss of generality.

The correlation function of the electric and magnetic energies can be deduced as:

$$C_{W_E}^{FF} \equiv \frac{\langle[W_E(\rho_1) - \langle W_E(\rho_1)\rangle]\,[W_E(\rho_2) - \langle W_E(\rho_2)\rangle]\rangle}{\sqrt{\langle[W_E(\rho_1) - \langle W_E(\rho_1)\rangle]^2\rangle\langle[W_E(\rho_2) - \langle W_E(\rho_2)\rangle]^2\rangle}} \tag{10}$$

$$C_{W_H}^{FF} \equiv \frac{\langle[W_H(\rho_1) - \langle W_H(\rho_1)\rangle][W_H(\rho_2) - \langle W_H(\rho_2)\rangle]\rangle}{\sqrt{\left\langle[W_H(\rho_1) - \langle W_H(\rho_1)\rangle]^2\right\rangle\langle[W_H(\rho_2) - \langle W_H(\rho_2)\rangle]^2\rangle}} \tag{11}$$

For stationary stochastic signals, the spatial correlation functions for the total field X_t exhibit a $SinC(k\rho)$ law.

$$C_{X_t}^{FF}(\rho) = \propto SinC(k\rho) \tag{12}$$

The spatial correlation functions of the transverse components X_t can be expressed as:

$$C_{X_t}^{FF}(\rho) = \frac{3}{2}\left\{SinC(k\rho) - \frac{1}{(k\rho)^2}\left[SinC(k\rho) - \kappa SinC\left(\frac{k\rho}{2}\right)\right]\right\} \tag{13}$$

where it can be established that $\kappa = cos\left(\frac{k\rho}{2}\right)$.

The $SinC(k\rho)$ law can be implemented using advanced signal processing convolutional accelerators based on broadband expansions:

$$SinC(k\rho) = \frac{Sin(k\rho)}{k\rho} = \sum_{n=1}^{n=\infty}(-1)^n \frac{(k\rho)^{2n}}{(2n+1)!} \tag{14}$$

$$SinC(k\rho) = \prod_{k=1}^{\infty} cos\left(\frac{k\rho}{2^k}\right) \tag{15}$$

The proposed SinC-based convolutional signal processing enables effective unification [4] of modeling and measurement techniques into a coherent framework. The benefits of unifying and aligning measurement (instrumentation) and modeling (EDA tooling) platforms go beyond the simple need for productivity enhancement, and they open new perspectives for transforming apparent antagonisms between theory and experiment into necessary complementarities [2,15]. Such complementarities will render possible introducing in the universe of simulations the notions of uncertainties usually considered as specific to the world of measurement. Although significant research efforts have been directed towards building accurate numerical algorithms dealing with modeling of uncertainties with controlled numerical errors, lack of knowledge in exact numerical values to assign to input parameters (design parameters, boundary and environmental conditions, etc.) has put constraints in their effective usage. The uncertainties are not only the results of our partial or insufficient knowledge of the mechanisms underlying the true physics; they also reflect various types of errors. In order to adopt variation-aware modeling methodologies, it is essential to include uncertainty analysis in simulations from the beginning and not in a posttreatment procedure. This requires stochastic computations either at the level of the handled operators or through techniques such as Monte Carlo and sampling methods or even by means of perturbation techniques, moment equations, etc. Among advantages of stochastic methods, over classical deterministic and sensitivity approaches that focus their analysis on the variability of individual parameters, are their abilities to consider the sets of observable parameters as main objects of investigation. The stochastic approach is built on the hypothesis of randomly distributed input parameters which imposes, from a theoretical point of view, using σ-algebra and associated measure to build a probability space. Numerical methods for stochastic [4] computations offer interesting possibilities for sensitivity and variability analysis. With sensitive or ill-conditioned problems, uncertainty in the input parameters can result in uncontrolled variations of the operators describing the governing equations. The powerful concept of stochastic Green's operators [2] provides solid foundations for bridging modeling and measurement into a unified framework.

3. Correlation-Based Power and Energy-Density Metrics for OTA-Testing of Mobile Devices

An antenna array module for mobile phones compliant with the 5G NR FR2 band in Europe is used as DUT. The unitary antenna element composing the array is based on the aperture-coupled structure introduced in [16]. A 4×4 mm^2 patch is placed 2 mm above the upper slot introducing an additional resonance, which allows the single-element bandwidth and gains to be increased. The antenna module is connectorized (see Figure 2a)

for a 4-Port measurement configuration using both frequency and time-domain instruments with and without down-conversion to sub-6 GHz frequency bands. Figure 2d depicts the area of the DUT used for near-field scanning of magnetic (H) and electric (E) fields with the associated power-density as a function of power levels.

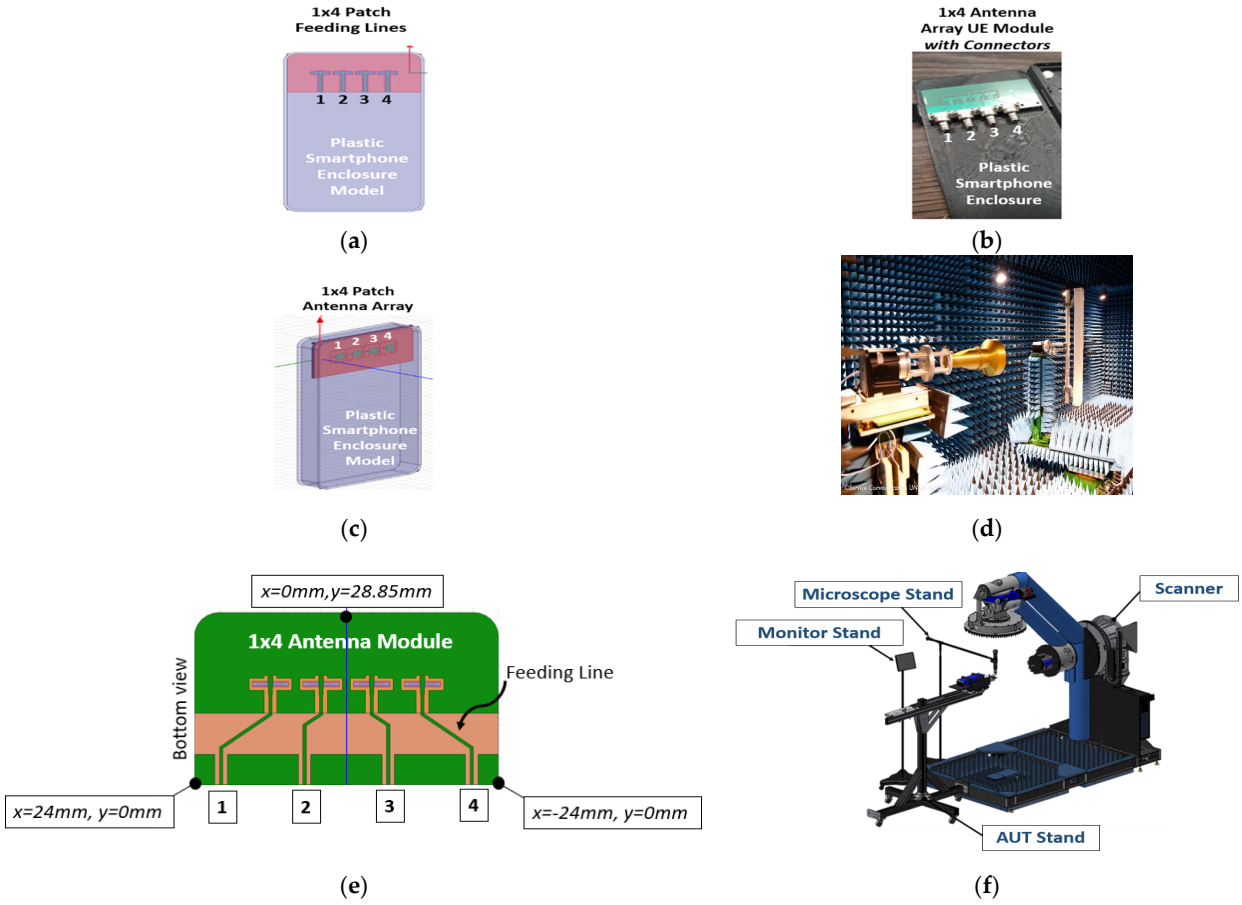

Figure 2. Experimental 26 GHz DUT with connectorized 1×4 antenna array in user equipment (**a**) and associated 3D model including enclosure (**b**) and feeding lines (**c**) built using full-wave solvers in time and frequency domains. DUT near-field scanning area for power and energy density measurement (**e**). Three-dimensional near-field (**d**) and far-field OTA scanning (**f**) solutions.

Figure 2d,f shows the experimental setup for 3D near-field and far-field OTA scanning systems.

The single-element S11 ≤ -10 dB impedance bandwidth is from 24.25 to 27.5 GHz, as shown in Figure 3 comparing measurement and simulations using 3D full-wave solvers.

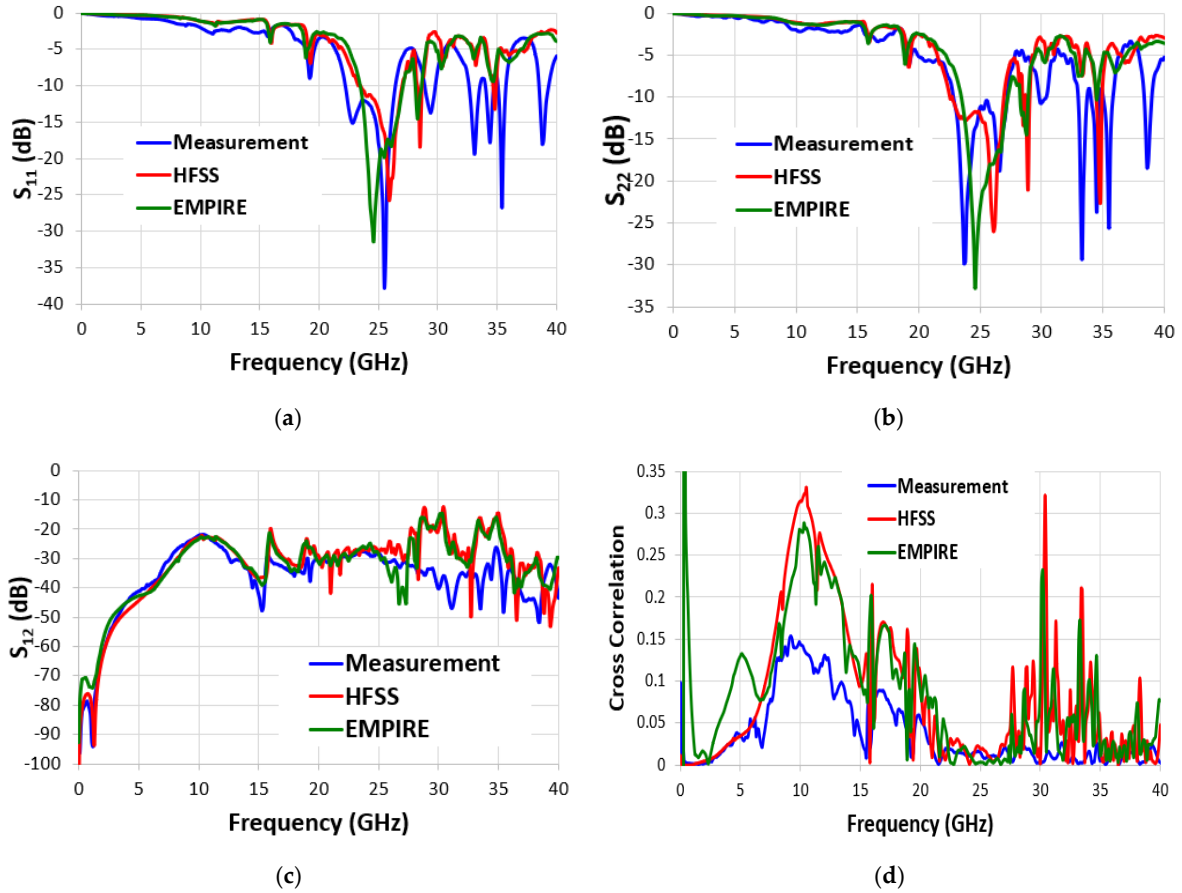

Figure 3. Broadband measurement of return-losses S11 (**a**), S22 (**b**) and near-coupling S12 (**c**) of the antenna elements compared to 3D full-wave simulations. Measured correlation functions (**d**) versus 3D full-wave simulations as function of frequency.

In Figure 4, the longitudinal, transverse, and total correlation functions are shown as a function of the $SinC(k\rho)$ law approximation order. It is observed that only a few numbers of terms are required to reach very accurate estimations (below 1% uncertainties for near-field OTA sensing).

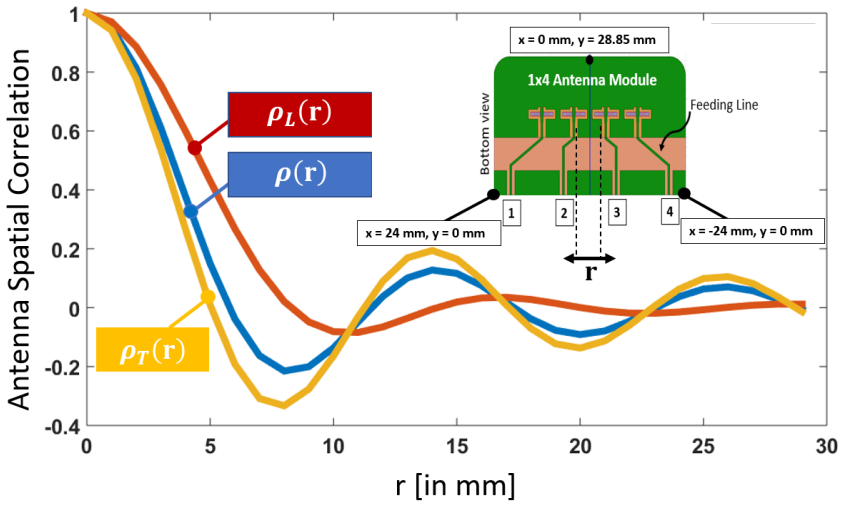

Figure 4. Transverse, longitudinal and total antenna spatial correlation as a function of the separation distance r between array elements.

Figure 5 shows the simulated (*using 3D EM solvers: IMST-EMPIRE, HFSS, CST*) three components of the magnetic and electric fields at 2 mm from the DUT for 15 dBm input power. The power density measured using EO probing is presented in Figure 6a at 10mm from the DUT. Ten millimeters is about a wavelength (λ), which corresponds to a distance where the extracted wave-impedance is very close (~99%) to 120 Ω (Figure 6b).

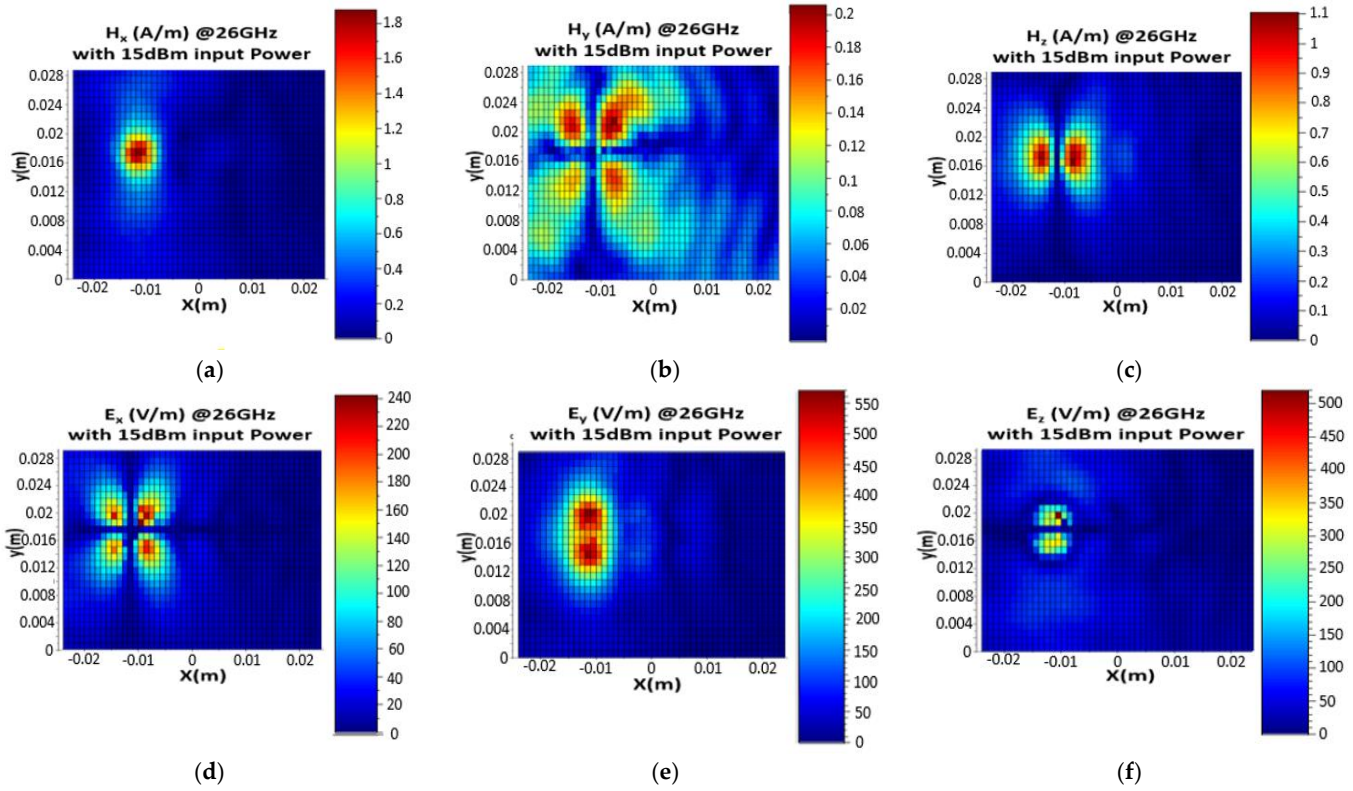

Figure 5. Magnetic field (**a**–**c**) and electric field (**d**–**f**) x, y and z components in near-field (2 mm from the DUT) at 26 GHz for 15 dBm input power.

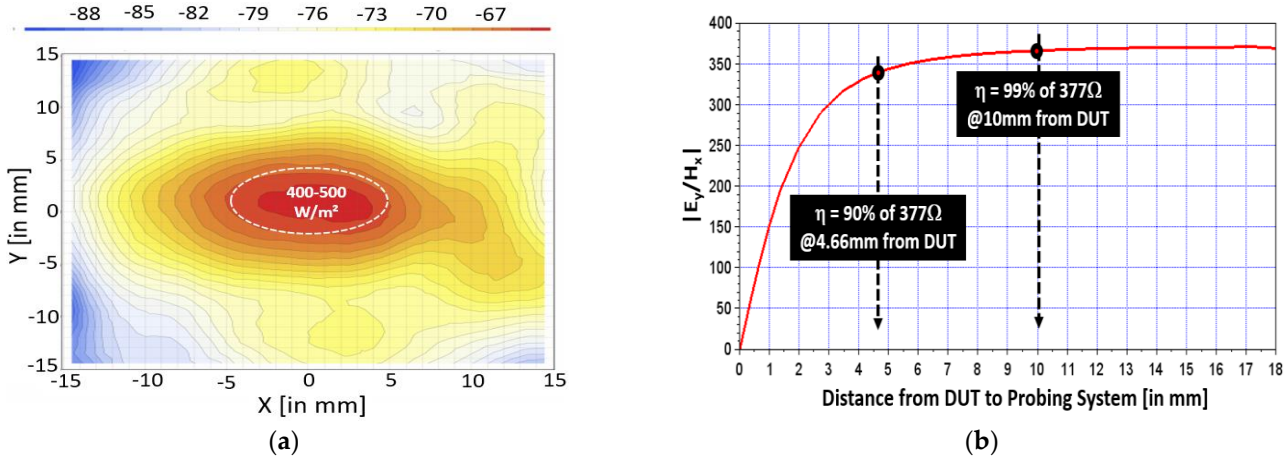

Figure 6. Measured power density at 26 GHz using electro-optical (EO) probing (**a**) and field-based extraction of wave-impedance (**b**) as function of distance between the DUT and the electro-optical probing.

With $E_i(\theta, \varphi)$ and $E_j(\theta, \varphi)$ being the radiation patterns of antennas 1 and 2, respectively, the envelope cross-correlation between the two antennas i and j expressed in the frequency-domain is given by the following equation:

$$\rho_E(\omega) = \frac{\left|\int_{4\pi} d\Omega\, E_i(\theta, \varphi) \cdot E_j^*(\theta, \varphi)\right|}{\sqrt{\int_{4\pi} d\Omega |E_i(\theta, \varphi)|^2} \sqrt{\int_{4\pi} d\Omega \left|E_j(\theta, \varphi)\right|^2}} \tag{16}$$

When using the S-parameters, the envelope cross-correlation [17–19] can be expressed as:

$$\rho_S(\omega) = \frac{\left|S_{ii}^*(\omega) S_{ij}(\omega) + S_{ji}^*(\omega) S_{jj}(\omega)\right|}{\sqrt{1 - |S_{ii}(\omega)|^2 - \left|S_{ji}(\omega)\right|^2} \sqrt{1 - \left|S_{jj}(\omega)\right|^2 - \left|S_{ij}(\omega)\right|^2}} \tag{17}$$

The normalizing loss-factor in Equation (18) is linked to radiation patterns information: when η_1 and η_2 denote the radiation efficiencies of antennas 1 and 2, S-parameters based envelope correlation can be cast in the following form:

$$\rho_S^{\eta_i - \eta_j}(\omega) = \frac{\rho_S(\omega)}{\sqrt{(1 - \eta_i)} \sqrt{(1 - \eta_j)}} \tag{18}$$

Relation (17) results in inequality as a consequence of uncertainties related to the actual value of the correlation of losses. Through the power conservation principle, the pattern orthogonality coefficient can be estimated from the scattering parameters for lossless antenna arrays. For lossy antenna arrays, because of losses in a decoupling network, the scattering parameters are incomplete [17–19] to calculate pattern orthogonality. In Figure 7, S-parameters-based cross-correlation and field–field-based cross-correlation functions extracted between antenna i and antenna j are presented, showing very good agreement over a broad frequency band. When the correlations between antenna i and antenna j are extracted, all other antenna elements are loaded by 50 Ω condition. Observed differences between S-parameters port-to-port-based cross-correlation and field–field-based cross-correlation functions in the band 20–30 GHz are attributed to imperfect load matching conditions and radiation losses [18,19] not easy to capture in S-parameters based definitions.

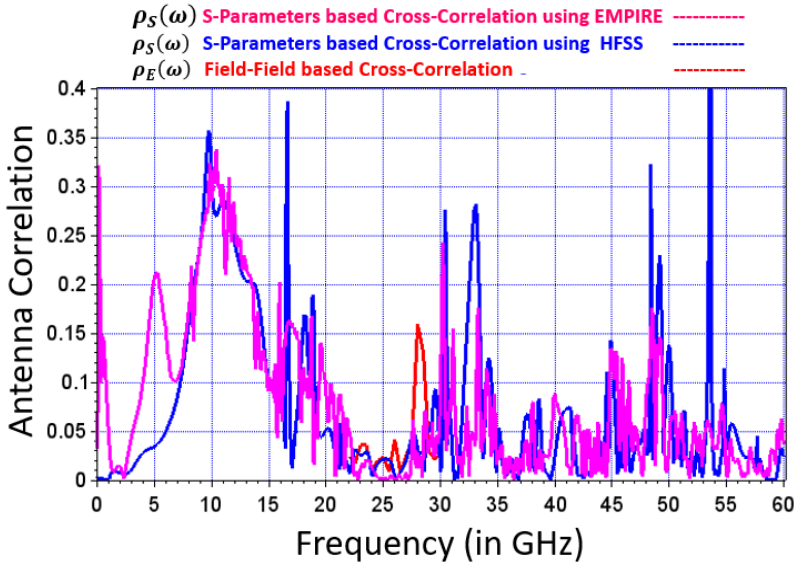

Figure 7. Comparisons between S-parameters port-to-port cross-correlation and field–field cross-correlation as function of frequency.

Measured power-density (Figure 8) in the near-field (10 mm) using EO [20] probing (with different antenna-factor (AF) values) with variable sensitivity from the DUT at 26 GHz with 23 dBm input power are compared to 3D full-wave EM simulations (CST, EMPIRE, HFSS) in time and frequency domains. Integral representation is used to derive spatial correlation functions for the complex electric and magnetic field components and total energy densities. The propagation of correlation [21] functions discriminating longitudinal and transverse directions of electric and magnetic field components in the near- and far-field lead to new algorithmic solutions (correlation ready convolutional signal-processing at FPGA level) for proper extraction of power-density and energy-density of wireless devices accounting for DUT to probing system interactions. Figure 9a,b represent the power-density as a function of distance from the DUT.

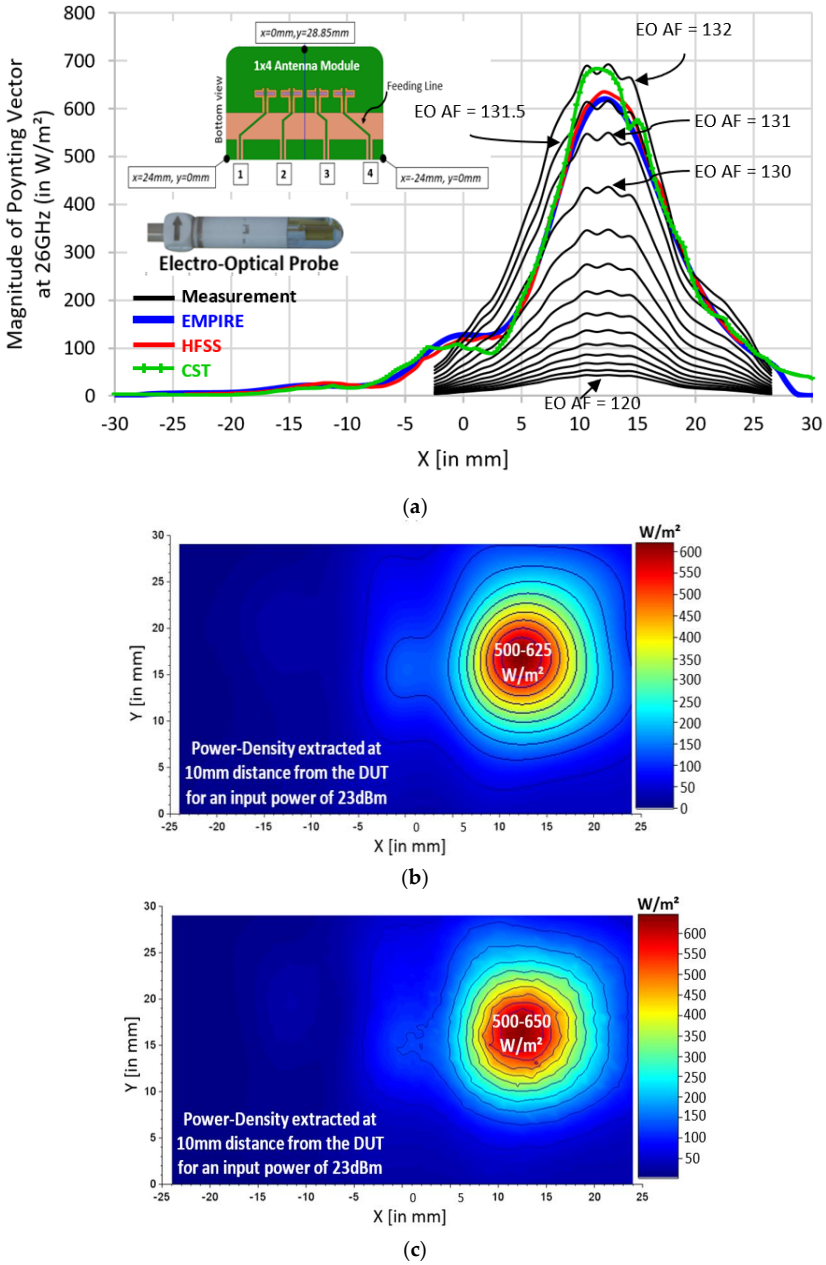

Figure 8. Measured (**a**) power-density as function of electro-optical (EO) probe sensitivity (from 132 dB/m to 120 dB/m) at 26 GHz: comparison with 3D full-wave EM solvers (CST (**a**), EMPIRE (**b**) and HFSS (**c**)).

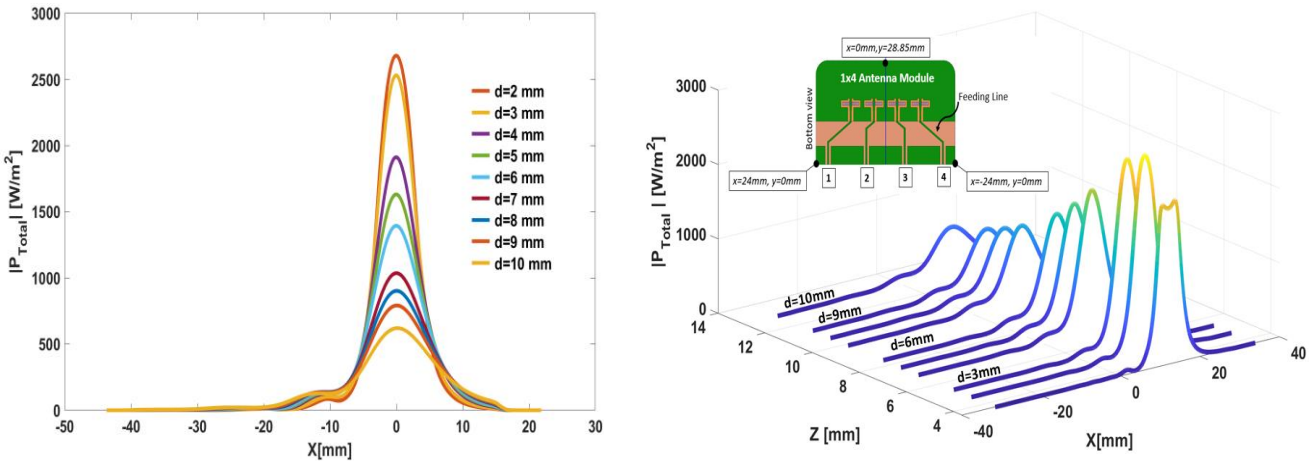

(**a**) (**b**)

Figure 9. Extracted power-density (**a**), (**b**) as function of probing distance.

In the time domain, the auto-correlation (AC) of signal $I_{S_i}(antenna\ i)$ and cross-correlation (CC) functions of signals I_{S_i} and $I_{S_j}(antenna\ j)$ can be extracted using the following expressions [21]:

$$AC_{I_{S_i}I_{S_i}}(\tau) = \lim_{T\to\infty} \frac{1}{2T} \int_{-T/2}^{+T/2} I_{S_i}(t) I_{S_i}(t+\tau) dt \tag{19}$$

$$CC_{I_{S_i}I_{S_j}}(\tau) = \lim_{T\to\infty} \frac{1}{2T} \int_{-T/2}^{+T/2} I_{S_i}(t) I_{S_j}(t+\tau) dt \tag{20}$$

The extraction of the auto-correlation and cross-correlation functions can be automated using eV-Technologies RF and mmWave correlator modules (Figure 10a) with embedded FPGA processing capabilities. The combination of eV-Technologies RF and mmWave correlator modules with optically synchronized dual-port instruments (Figure 10b) opens new possibilities for OTA-based interferometric [22,23] measurement (including correlation-based EVM testing [24]) of MIMO applications using minimally invasive probing solutions [20].

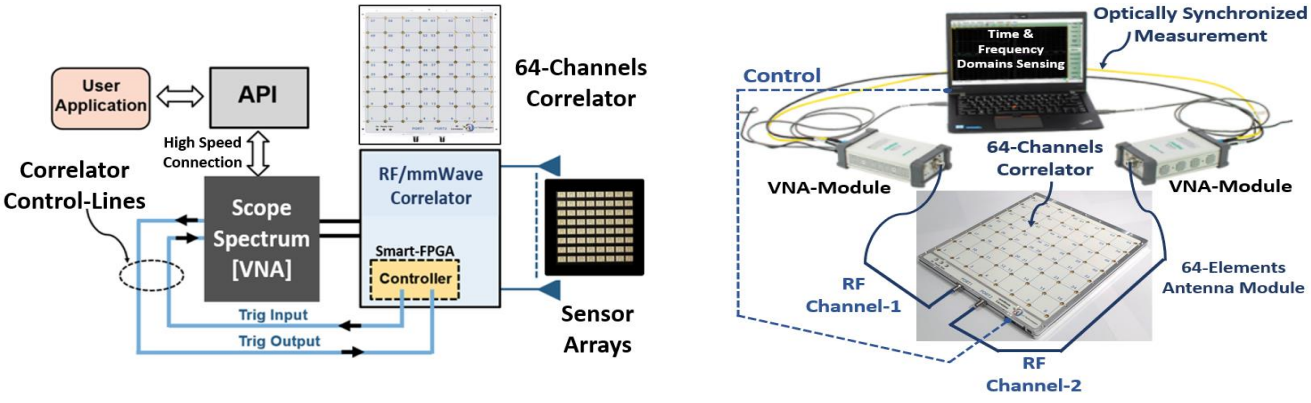

(**a**) (**b**)

Figure 10. 64-Channels correlator (**a**) module combined with 64 broadband sensor-array elements. Optically synchronized VNA modules for broadband extraction of correlation functions (**b**).

4. Perspectives for Unified Information Signal Theory (IT) and Physical Information Theory (PT) Using Correlation Technologies

Stochastic noise-aware [25–32] approaches create natural bridges between correlation formalisms and convolutional techniques. Linking correlation to convolution will enable combining information signal theory (IT) and physical information theory (PT) into a unified approach. Such a unified approach can be established in the general scope of the fluctuation–dissipation theorem (FDT) [25] envisaged as a cornerstone for bridging noise mechanisms with the retrieval of Green's functions through the formalism of auto and cross-correlation operators.

The cross-correlation function $C_{AB}(\tau)$ of stationary stochastic signals $S_A(t)$ and $S_B(t)$ is defined by the following equation, where the brackets denote the ensemble average:

$$\begin{aligned} C_{AB}(\tau) &= S_A(t)|S_B(t+\tau) \\ &= \lim_{T\to\infty} \tfrac{1}{2T} \int_{-T/2}^{+T/2} S_A(t)S_B(t+\tau)dt \end{aligned} \tag{21}$$

The correlation matrix in the frequency domain can be expressed as a function of the time-windowed signal $S_T(t)$:

$$C(\omega) = \mathcal{F}\{\langle S_T(t) \Big| S_T^{\dagger}(t+\tau) \rangle\} \tag{22}$$

The superscript † refers to the Hermitian conjugate operation.

For a given frame, the power spectra of the signals can be deduced from the correlation matrix C(t):

$$C(t) = \begin{pmatrix} C_{11}(t) & C_{12}(t) & \dots & C_{1N}(t) \\ C_{21}(t) & C_{22}(t) & \dots & C_{2N}(t) \\ \vdots & \vdots & \dots & \vdots \\ C_{N1}(t) & C_{N2}(t) & \dots & C_{NN}(t) \end{pmatrix} \tag{23}$$

Assuming signals and noise contributions are uncorrelated, by applying the Expectation operator E[.], the following relations can be derived:

$$\begin{aligned} E\left[(S_A + N_A)\overline{(S_A + N_B)}\right] &= E\left[|S_A|^2\right] + E\left[S_A\overline{N_B}\right] + E\left[N_A\overline{S_A}\right] + E\left[N_A\overline{N_B}\right] \\ &= P_{S_A} + P_{Noise} \end{aligned} \tag{24}$$

where is the P_{S_A} and P_{Noise} are respectively the signal (channel A) and noise powers.

In (24) S_A and S_B refer to the signals at access terminals (or channels) A and B, and N_A and N_B are the noise contributions on channels A and B. This equation clearly shows that uncorrelated noise contributions are totally eliminated.

Thus, the uncorrelated noise power is removed based on the cross-correlation, however the signal power and the correlated noise power are not removed. As a result, the removal of the uncorrelated noise power improves the SNR, and therefore renders possible detecting signals with lower energy levels.

The use of microscopic correlations to obtain the macroscopic entropy for an equilibrium system was studied by Lindgren in [29]. The conventional definition of the physical entropy S of a system with a particular microstate—e.g., energy, composition, volume, (U,N,V)—in statistical physics and that of information H(z), can be linked by the following equation adopting the notation in [30]:

$$H(z) = S(U,N,V)/k\ln(2) = -\sum_{s} P_z(s)\log_2 P_z(s) \tag{25}$$

The Shannon–McMillan–Breiman theorem provides a formal bridge [31] between the Boltzmann entropy and the Shannon entropy. In (25), the average information in a set of messages associated with probabilities $P_z(s)$ map onto the ensemble of the microstates

of the physical system. The variable z is a label for the set of possible messages, and the probability over this set, s is a particular value from the set. Equation (25) being valid in the case of non-equilibrium systems, for a well-defined ensemble probability distribution, $P_z(s)$, several conceptual difficulties arise from the physical interpretation of system complexity in link with equilibrium entropy. These conceptual difficulties reveal the dependence of entropy on the scale [30] of analysis. The concept of a scale-dependent entropy dates back to the ε-entropy of Kolmogorov [32], which can be linked to Shannon noisy-channel information theory [33]. Multi-scale analysis of the structure of the state space relates the energy, entropy, and geometry at different levels of resolution for both equilibrium and non-equilibrium conditions. For dynamic systems in non-equilibrium conditions, the use of entropy-based [34] metrics for evaluating the attributes of chaotic regimes will open new possibilities. In [35], it is suggested that for any bounded system with entropy $S_{Entropy}$ and rest energy ERest, there exists a universal upper limit on the entropy-to-energy ratio, which leads to the following inequality:

$$S_{Entropy} / E_{Rest} \leq 2\pi R \tag{26}$$

where R represents the radius of the sphere circumscribing the system. For topologically compact systems, R is to be defined in terms of the system's volume. In the derivation of (26) we have assumed $h/2\pi = k = G = 1$ without loss of generality.

In [36], the implications of the entropy-to-energy ratio on an upper bound of the entropy-to-surface-area ratio are discussed. The resulting entropy-to-surface-area ratio is expressed in the form:

$$S_{Entropy} / A_{Surface} \leq \frac{1}{4} \tag{27}$$

The limit of (26) leads to the equality $S_{Entropy} = A_{Surface}/4$, which is consistent with the expression for black holes.

The derived entropy-to-energy and entropy-to-surface-area bounds open new possibilities in communication theory for properly coupling IT and PT into a unified approach.

In reference to computational energy dissipation, Landauer, in 1961, has stated the principle that erasing one bit of information entails an energy loss of kTln(2) (the thermodynamic threshold), where k is the Boltzmann constant and T is the temperature in Kelvin. This principle has generated rich comments [37] and motivated new directions of ambitious research solutions (e.g., applied superconductivity [38]) with less dissipation than the Landauer limit.

Figure 11a shows technology trends [39] expressed in terms of dissipated energy per operation in reference to the Landauer limit. Figure 3a presents the power consumption as a function of bit rates and computing power versus dissipated energy in J/bit. Following Moore's exponential trend, the energy efficiency of a transistor and a logic gate has improved by a factor of one hundred in ten years, corresponding to a factor of two every 18 months. The trends of Moore's prediction are starting to show some saturation as the exponential decrease in the physical size of the transistor is constrained by the physical limits. At the lower scales, the switching energy is approaching the thermal noise spectral density. In addition, the cooling capacity in terms of energy per unit time for a given area will lead to a bottleneck imposing energy–geometry–entropy trade-offs [39].

Energy–Geometry–Entropy trade-offs will foster new signal processing solutions taking advantage of the stochastic resonance (SR) concept for low-power operating communication systems. Although noise is generally considered a nuisance, in certain conditions, by exploiting the concept of stochastic resonance [40–42], noise can enhance the detection of weak signals. The attribute of stochastic resonance is that the signal-to-noise ratio (SNR), following the general formula [40] in Equation (28), is zero for zero added noise (that is, $D \rightarrow 0$: no noise implies no switching or threshold crossings, thus no output), increases sharply to a maximum at some optimal noise intensity.

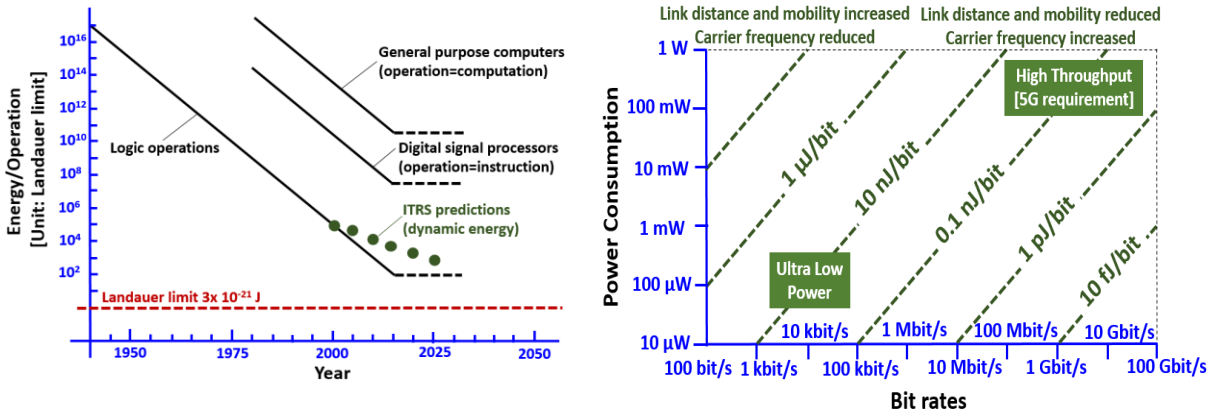

(**a**) (**b**)

Figure 11. Technology trend (**a**) of dissipated energy per operation expressed in reference to Landauer limit against evolution over years showing saturation effects, power consumption versus bit rate (**b**).

In Equation (28), ε is the input signal strength, D is the input noise intensity, and ΔU is a constant related to the barrier height or the threshold.

$$\mathrm{SNR} \propto \left(\frac{\varepsilon \Delta U}{D}\right)^2 \mathrm{Exp}\left(\frac{\Delta U}{D}\right) \tag{28}$$

The idea of using a narrow-band random noise as a carrier for information transmission was proposed by Rowe in his papers [43,44] published in 1964. With stochastic carriers, a high SNR can be obtained when the modulation bandwidth is relatively limited.

The optimization of SNR for stochastic signals requires proper extraction of spectral power density. Since the power spectral density and autocorrelation are a Fourier transform pair, there is a strong link between correlations and SNR.

Although Fourier transforms cannot be established rigorously for random processes (infinite energy), they can nevertheless be derived for the autocorrelation and cross-correlation functions which are non-periodic energy signals. The Fourier transforms of the correlation is called power spectrum or spectral density function (SDF).

In the practical case of the 3-Port power-splitter structure in Figure 12a, the temporal power of the combined signal $S_3(t)$ in Figure 12a can be cast in the following form assuming a time delay of τ_D in the presence of noise:

$$\begin{aligned} P_{S_3} = \lim_{t\to\infty} \tfrac{1}{2T} \int_{-T}^{T} \left(S_3^2(t)\right) dt = \tfrac{1}{2} \lim_{t\to\infty} \tfrac{1}{2T} \int_{-T}^{T} [(S_1(t)) + S_1(t-\tau_D) + n_1(t) + n_2(t)]^2 dt \\ = \tfrac{1}{2} \lim_{t\to\infty} \tfrac{1}{2T} \int_{-T}^{T} \{[S_1(t) + S_1(t-\tau_D)]^2 + \\ 2[(S_1(t)) + S_1(t-\tau_D)][n_1(t) + n_2(t)] + \\ [n_1(t) + n_2(t)]^2\} dt \end{aligned} \tag{29}$$

$n_1(t)$ and $n_2(t)$ represent the noise in the two channels. The accuracy of the broadband power power-splitters is essential for the avoidance of squint and impairments in phased-array systems. Integration of the binomial for the signal and noise contributions leads to the following expressions:

$$[S_1 + S_1(t-\tau_D)]^2 = S_1^2(t) + 2S_1(t)S_2(t) + S_1^2(t-\tau_D) \tag{30}$$

$$[n_1(t) + n_1(t)]^2 = n_1^2(t) + n_2^2(t) + 2n_1(t)n_2(t) \tag{31}$$

The resulting power of the combined signal is twice the power of the reference signal $S_1(t)$ plus twice its autocorrelation power:

$$P_{S_3}(\tau_D) = \alpha^2\left(\, 2P_{S_1} + 2R_{Autocorr}(\tau_D)\right) \tag{32}$$

where α is relative to the power splitting factor.

Assuming a band-limited filtering $f_1 - f_2$ the autocorrelation function takes the following simplified form:

$$R_{Autocorr}(\tau_D) = P_{S_1} cos(\pi(f_1 + f_2)\tau_D)\frac{sin(\pi(f_1 - f_2)\tau_D)}{\pi(f_1 - f_2)\tau_D} \tag{33}$$

In the case of complex I-Q correlators, the real and imaginary parts can be obtained from the following equations based on the synoptic bloc diagram shown in Figure 12 with DC offset compensation [45]:

$$R = R_0 sinc\left[B(\tau_g - \tau_i)\right] cos\left\{2\pi\left[\omega_{LO}\tau_g - \omega_{IF}(\tau_g - \tau_i)\right] + \varphi_{LO}\right\} \tag{34}$$

$$I = R_0 sinc\left[B(\tau_g - \tau_i)\right] sin\left\{2\pi\left[\omega_{LO}\tau_g - \omega_{IF}(\tau_g - \tau_i)\right] + \varphi_{LO}\right\} \tag{35}$$

τ_g and τ_i are the time delay presented at RF and IF between the two receivers.

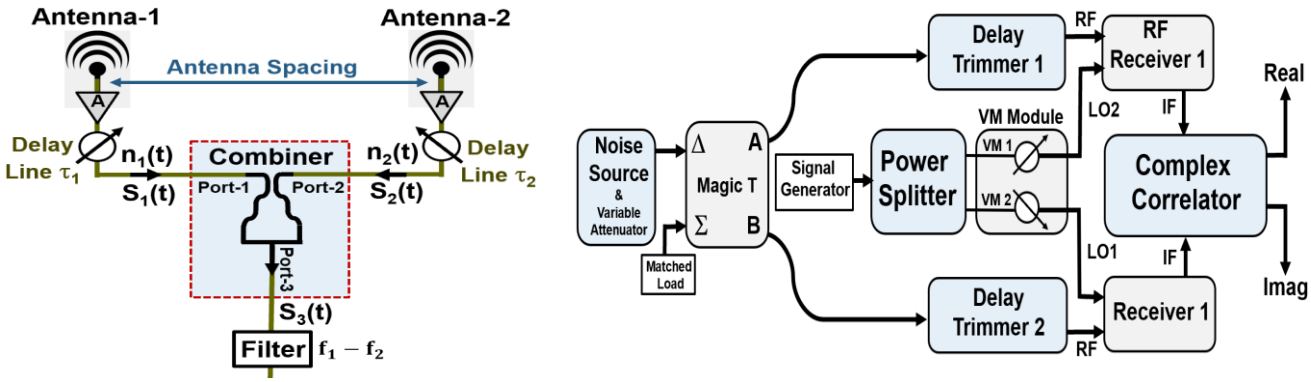

Figure 12. Dual-channel with delay lines and power-splitting for noise decorrelation (**a**). Test-bench solution including broadband delay lines and power-splitters for noise decorrelation using IQ signals (**b**).

5. Conclusions

In this paper, we have presented correlation technologies for measuring the power density of mobile devices using OTA testing. Measurements obtained using minimally invasive electro-optical (EO) probes are compared to full-wave 3D EM solvers (EMPIRE, HFSS, CST), demonstrating excellent agreement for applications at mmWave frequencies.

New ASIC-embedded smart connectors are developed for bringing correlation-based signal processing close to antenna modules. The influence of separation distance between the device under test (DUT) and the probing system (PS) is studied using spatial correlation functions and their propagation attributes implemented through FPGA programming based on convolutional algorithms (*cognition ready array-processing*). Proposed correlation-based energy-density and power-density metrics in providing stronger robustness to noise represent valuable insights to mobile equipment manufacturers, network operators, and standardization bodies. Perspectives for optically synchronized interferometric correlation technologies are drawn for accurate measurements in noisy environments of stochastic EM fields using power-spectra, energy-spectra, and entropy metrics. At baseband frequencies, ongoing work is relative to new DSP-based convolutional accelerators compliant with IEEE

P1765 standard for pushing EVM [24] measurement solutions to industrial testing both in connectorized and OTA configurations using correlation technologies. Implementation of DSP-based convolutional accelerators into advanced FD-SOI-ASIC platforms for co-integration with adaptive RF/mmWave front-end modules will enable real-time extraction of auto-correlation and cross-correlation functions of stochastic signals for mobile devices and systems.

The proposed correlation technologies will enable an efficient combination of information signal theory (IT) and physical information theory (PT) into a unified approach: *Shannon's entropy* can be directly related to *Boltzmann's entropy*. The Shannon–McMillan–Breiman theorem [31] provides a formal basis for such a unified approach where Shannon's entropy can be directly related to Boltzmann's entropy for accurate extraction of key parameters characterizing the quality of RF wireless systems such as signal-to-noise ratio (SNR), Error Vector Magnitude (EVM), channel capacity (CA), data rate (DR) and antennas tuning in MIMO applications.

Beyond classical RF applications, proposed correlation technologies will foster new perspectives in creating natural bridges between "Correlation" and "Intrication", in the quantum-physics sense, that can be leveraged for future Qubit-based coding, encryption, and signal-processing. Quantum computing and quantum radar [46–58] sensing-related applications will benefit from such holistic correlation technologies [59–61]. Spintronics-based sensing solutions introduced in [61] will enable new correlation-aware wireless communication systems.

Author Contributions: Conceptualization, S.W.; methodology, S.W. Validation Measurement versus 3D Modeling of DUT, F.F., T.V.D., D.B.; Measurement using EO Probing, L.D., G.G.; writing—original draft preparation, S.W.; writing—review and editing, S.W.; DSP and FPGA analysis, V.H. All authors have read and agreed to the published version of the manuscript.

Funding: This research was funded by eV-Technologies.

Acknowledgments: The authors are very grateful to Jacques Sombrin for ongoing work on Correlation-based EVM measurement of MIMO systems.

Conflicts of Interest: The authors declare no conflict of interest.

Abbreviations

The following abbreviations are used in this manuscript:

FF-CF	Field–Field correlation functions
OTA	Over-The-Air
ASIC	Application Specific Integrated Circuit
EVM	Error Vector Magnitude
DSP	Digital Signal Processing
FD-SOI	Fully Depleted Silicon-On-Insulator
EO	Electro-Optical

References

1. Hill, D.A. Spatial correlation function for fields in a reverberation chamber. *IEEE Trans. Electromagn. Compat.* **1995**, *37*, 138. [CrossRef]
2. Wane, S. Power Integrity, Signal Integrity, EMI & EMC in Integrated Circuits and Systems: Towards Multi-Physics Energy-Oriented Approaches. Habilitation à Diriger des Recherches Thesis, Institut National Polytechnique de Toulouse (INPT), Caen, France, 2013.
3. Gradoni, G.; Ramapriya, D.M.; Creagh, S.C.; Tanner, G.; Baharuddin, M.H.; Nasser, H.; Smartt, C.; Thomas, P.D.W. Near-field scanning and propagation of correlated low-frequency radiated emissions. *IEEE Trans. Electromagn. Compat.* **2017**, *60*, 2045–2048. [CrossRef]
4. Wane, S.; Patton, R.; Gross, N. Unification of instrumentation and EDA tooling platforms for enabling smart chip-package-PCB-probe arrays co-design solutions using advanced RFIC technologies. In Proceedings of the 2018 IEEE Conference on Antenna Measurements & Applications (CAMA), Västerås, Sweden, 3–6 September 2018; pp. 1–4.

5. Weaver, R.L.; Lobkis, O.J. Ultrasonics without a Source: Thermal Fluctuation Correlations at MHz Frequencies. *Phys. Rev. Lett.* **2001**, *87*, 134301. [CrossRef]
6. Roux, P.; Kuperman, W.A. Extracting coherent wavefronts from acoustic ambient noise in the ocean. *J. Acoust. Soc. Am.* **2004**, *116*, 1995–2003. [CrossRef]
7. Rickett, J.; Claerbout, J.F. Acoustic daylight imaging via spectral factorization; helioseismology and reservoir monitoring. *Lead. Edge* **1999**, *18*, 957–960. [CrossRef]
8. Snieder, R.; Wapenaar, K.; Wegler, U. Unified Green's function retrieval by cross-correlation; connection with energy principles. *Phys. Rev. E* **2007**, *75*, 036103. [CrossRef] [PubMed]
9. Fourestie, B.; Bolomey, J.-C.; Sarrebourse, T.; Altman, Z.; Wiart, J. Spherical near field facility for characterizing random emissions. *IEEE Trans. Antennas Propag.* **2005**, *53*, 2582–2589. [CrossRef]
10. Wolf, E. New theory of partial coherence in the space–frequency domain. Part I: Spectra and cross spectra of steady-state sources. *J. Opt. Soc. Am.* **1982**, *72*, 343–351. [CrossRef]
11. Glauber, R.J. The Quantum Theory of Optical Coherence. *Phys. Rev.* **1963**, *130*, 2529–2539. [CrossRef]
12. Urkowitz, H. Energy detection of unknown deterministic signals. *Proc. IEEE* **1967**, *55*, 523–531. [CrossRef]
13. Ferreira, D.; Bachelard, R.; Guerin, W.; Kaiser, R.; Fouché, M. Connecting field and intensity correlations: The Siegert relation and how to test it. *Am. J. Phys.* **2020**, *88*, 831–837. [CrossRef]
14. Harrington, R.F. *Time-Harmonic Electromagnetic Fields*; McGraw-Hill: New York, NY, USA, 1961.
15. Derat, B.; Celik, M.; Schmitz, S.; Simon, W.; Lauer, A. Toward Augmented OTA Testing: Bringing Full-Wave Numerical Modeling and Antenna Measurements Together. *Microw. J.* **2021**, *64*, 56–68.
16. Nguyen, T.Q.K.; Miah, M.S.; Lizzi, L.; Haneda, K.; Ferrero, F. Experimental evaluation of user's finger effects on a 5G terminal antenna array at 26 GHz. *IEEE Antennas Wirel. Propag. Lett.* **2020**, *19*, 892–896. [CrossRef]
17. Mikki, S.M.; Antar, Y.M.M. On Cross Correlation in Antenna Arrays With Applications to Spatial Diversity and MIMO Systems. *IEEE Trans. Antennas Propag.* **2015**, *63*, 1798–1810. [CrossRef]
18. Hallbjorner, P. The significance of radiation efficiencies when using S-parameters to calculate the received signal correlation from two antennas. *IEEE Antennas Wirel. Propag. Lett.* **2005**, *4*, 97–99. [CrossRef]
19. Wang, K.; Li, L.; Eibert, T.F. Estimation of Signal Correlation of Lossy Compact Monopole Arrays With Decoupling Networks. *IEEE Trans. Antennas Propag.* **2014**, *63*, 357–363. [CrossRef]
20. Behague, F.; Calero, V.; Coste, A.; Godet, A.; Suarez, M.; Gaborit, G.; Duvillaret, L.; Baida, F.I.; Bernal, M.-P.; Courjal, N. Minimally invasive optical sensors for microwave-electric-field exposure measurements. *J. Opt. Microsyst.* **2021**, *1*, 020902. [CrossRef]
21. Wane, S.; Dinh, T.V.; Tran, Q.H.; Bajon, D.; Ferrero, F.; Duvillaret, L.; Gaborit, G.; Sombrin, J.; de Lédinghen, E.; Laban, P.; et al. Correlation Technologies for OTA Testing of mmWave Mobile Devices Using Energy Metrics. In Proceedings of the 2022 IEEE Radio and Wireless Symposium (RWS), Las Vegas, NV, USA, 16–19 January 2022.
22. Craeye, C.; Withington, S.; Thomas, C.N. Characteristic functions describing the power absorption response of periodic structures to partially coherent fields. *J. Opt. Soc. Am. A* **2014**, *31*, 1360–1368. [CrossRef]
23. Tihon, D.; Withington, S.; Bailly, E.; Vest, B.; Greffet, J.-J. General relation between spatial coherence and absorption. *Opt. Express* **2021**, *29*, 425. [CrossRef]
24. Sombrin, J. On the formal identity of EVM and NPR measurement methods: Conditions for identity of error vector magnitude and noise power ratio. In Proceedings of the 2011 41st European Microwave Conference, Manchester, UK, 10–13 October 2011; pp. 337–340.
25. Kubo, R. The fluctuation-dissipation theorem. *Rep. Prog. Phys.* **1966**, *29*, 255–284. [CrossRef]
26. Nyquist, H. Thermal Agitation of Electric Charge in Conductors. *Phys. Rev.* **1928**, *32*, 110. [CrossRef]
27. Callen, H.B.; Welton, T.A. Irreversibility and Generalized Noise. *Phys. Rev.* **1951**, *83*, 34–40. [CrossRef]
28. Onsager, L. Reciprocal Relations in Irreversible Processes. I. *Phys. Rev.* **1931**, *37*, 405–426. [CrossRef]
29. Lindgren, K. Microscopic and macroscopic entropy. *Phys. Rev. E* **1988**, *38*, 4794–4798. [CrossRef] [PubMed]
30. Bar-Yam, Y. Dynamics of Complex Systems (Perseus, 1997), Chapters 8 and 9. Available online: https://necsi.edu/dynamics-of-complex-systems (accessed on 5 January 2022).
31. Lesne, A. Shannon entropy: A rigorous notion at the crossroads between probability, information theory, dynamical systems and statistical physics. *Math. Struct. Comput. Sci.* **2014**, *24*, 2–43. [CrossRef]
32. Shannon Entropy: A Rigorous Mathematical Notion at the Crossroads between Probability, Information Theory, Dynamical Systems and Statistical Physics. Available online: https://preprints.ihes.fr/2011/M/M-11-04.pdf (accessed on 5 January 2022).
33. Shannon, C.E. A Mathematical Theory of Communication. *ACM SIGMOBILE Mob. Comput. Commun. Rev.* **2001**, *5*, 3–55. [CrossRef]
34. Gradoni, G.; Primiani, V.M.; Moglie, F. Reverberation chamber as a statistical relaxation process: Entropy analysis and fast time domain simulations. In Proceedings of the International Symposium on Electromagnetic Compatibility—EMC EUROPE, Rome, Italy, 17–21 September 2012.
35. Bekenstein, J.D. Universal upper bound on the entropy-to-energy ratio for bounded systems. *Phys. Rev. D* **1981**, *23*, 287–298. [CrossRef]
36. PGonzález-Díaz, P.F. Bounds on the entropy. *Phys. Rev. D* **1983**, *27*, 3042–3043. [CrossRef]
37. Porod, W.; Grondin, R.O.; Ferry, D.K. Dissipation in computation. *Phys. Rev. Lett.* **1984**, *52*, 232–235. [CrossRef]

38. Ren, J.; Semenov, V.K. Progress With Physically and Logically Reversible Superconducting Digital Circuits. *IEEE Trans. Appl. Supercond.* **2011**, *21*, 780–786. [CrossRef]
39. Wane, S.; Bajon, D.; Russer, J.; Russer, P.; Gradoni, G. Energy-geometry-entropy bounds aware analysis of stochastic field-field correlations for emerging wireless communication technologies. In Proceedings of the 2017 XXXIInd General Assembly and Scientific Symposium of the International Union of Radio Science (URSI GASS), Montreal, QC, Canada, 19–26 August 2017.
40. Wiesenfeld, K.; Moss, F. Stochastic resonance and the benefits of noise: From ice ages to crayfish and SQUIDs. *Nature* **1995**, *373*, 33–36. [CrossRef]
41. Bulsara, A.; Jacobs, E.; Zhou, T.; Moss, F.; Kiss, L. Stochastic resonance in a single neuron model: Theory and analog simulation. *J. Theor. Biol.* **1991**, *152*, 531–555. [CrossRef]
42. Gammaitoni, L.; Martinelli, M.; Pardi, L.; Santucci, S. Observation of stochastic resonance in bistable electron-paramagnetic-resonance systems. *Phys. Rev. Lett.* **1991**, *67*, 1799–1802. [CrossRef] [PubMed]
43. Rowe, H. Amplitude modulation with a noise carrier. *Proc. IEEE* **1964**, *52*, 389–395. [CrossRef]
44. Rowe, H. Frequency or phase modulation with a noise carrier. *Proc. IEEE* **1964**, *52*, 396–408. [CrossRef]
45. Solbach, K. Noise Signal Decorrelation in Broad-Band Active Phased Array Systems. *Frequenz* **2001**, *55*, 317–322. [CrossRef]
46. Lloyd, S. Enhanced sensitivity of photodetection via quantum illumination. *Science* **2008**, *321*, 1463–1465. [CrossRef]
47. Tan, S.-H.; Erkmen, B.I.; Giovannetti, V.; Guha, S.; Lloyd, S.; Maccone, L.; Pirandola, S.; Shapiro, J.H. Quantum Illumination with Gaussian States. *Phys. Rev. Lett.* **2008**, *101*, 253601. [CrossRef]
48. Zhang, Z.; Tengner, M.; Zhong, T.; Wong, F.N.C.; Shapiro, J.H. Entanglement's Benefit Survives an Entanglement-Breaking Channel. *Phys. Rev. Lett.* **2013**, *111*, 010501. [CrossRef]
49. ELopaeva, E.D.; Ruo-Berchera, I.; Degiovanni, I.P.; Olivares, S.; Brida, G.; Genovese, M. Experimental Realization of Quantum Illumination. *Phys. Rev. Lett.* **2013**, *110*, 153603. [CrossRef]
50. Zhang, Z.; Mouradian, S.; Wong, F.N.C.; Shapiro, J.H. Entanglement-Enhanced Sensing in a Lossy and Noisy Environment. *Phys. Rev. Lett.* **2015**, *114*, 110506. [CrossRef]
51. Barzanjeh, S.; Guha, S.; Weedbrook, C.; Vitali, D.; Shapiro, J.H.; Pirandola, S. Microwave Quantum Illumination. *Phys. Rev. Lett.* **2015**, *114*, 080503. [CrossRef] [PubMed]
52. Gu, X.; Kockum, A.F.; Miranowicz, A.; Liu, Y.-X.; Nori, F. Microwave photonics with superconducting quantum circuits. *Phys. Rep.* **2017**, *718*, 1–102. [CrossRef]
53. Sanz, M.; las Heras, U.; Garcia-Ripoll, J.J.; Solano, E.; Di Candia, R. Quantum estimation methods for quantum illumination. *Phys. Rev. Lett.* **2017**, *118*, 070803. [CrossRef] [PubMed]
54. Zhuang, Q.; Zhang, Z.; Shapiro, J.H. Optimum Mixed-State Discrimination for Noisy Entanglement-Enhanced Sensing. *Phys. Rev. Lett.* **2017**, *118*, 040801. [CrossRef] [PubMed]
55. di Candia, R.; Yigitler, H.; Paraoanu, S.G.; Jntti, R. Two-way covert microwave quantum communication. *arXiv* **2020**, arXiv:2004.07192. [CrossRef]
56. Nair, R.; Gu, M. Fundamental limits of quantum illumination. *Optica* **2020**, *7*, 771–774. [CrossRef]
57. Chang, C.W.S.; Vadiraj, A.M.; Bourassa, J.; Balaji, B.; Wilson, C.M. Quantum-enhanced noise radar. *Appl. Phys. Lett.* **2019**, *114*, 112601. [CrossRef]
58. Barzanjeh, S.; Pirandola, S.; Vitali, D.; Fink, J.M. Microwave quantum illumination using a digital receiver. *Sci. Adv.* **2020**, *6*, eabb0451. [CrossRef] [PubMed]
59. Wane, S. ASIC-Correlators with Embedded Cognition for Smart OTA Test, EMC and OTA Tests of Wireless Devices in Reverberation Chambers, Europe 2021. Available online: https://www.emc2021.emcss.org/assets/images/emc2021FinalProgram.pdf (accessed on 5 January 2022).
60. Wane, S.; Ferrero, F.; Dinh, T.; Bajon, D.; Duvillaret, L.; Gaborit, G.; Tombakdjian, L.; Park, C.-S.; Craeye, C.; Huard, V.; et al. Correlation Technologies for OTA Testing of Mobile Devices: Power-Density Measurement. In Proceedings of the 2021 IEEE Conference on Antenna Measurements & Applications (CAMA), Antibes Juan-les-Pins, France, 15–17 November 2021.
61. Wane, S.; Tran, Q.; Dinh, T.; Terki, F.; Bajon, D.; Huard, V.; Nyssens, L.; Raskin, J.-P.; Lederer, D.; Eudeline, P.; et al. High Resolution Spintronics Probe-Array Technology Solutions for Very Near-Field Scanning. In Proceedings of the 2021 IEEE Conference on Antenna Measurements & Applications (CAMA), Antibes Juan-les-Pins, France, 15–17 November 2021.